Random waves in a vibrated 2D granular medium with magnetic dipolar interactions

Michael Berhanu[1], Simon Merminod[1,2], Éric Falcon[1] & Gustavo Castillo[3]

[1] Université Paris Diderot, MSC, UMR 7057 CNRS, Paris, France
[2] Martin Fisher School of Physics, Brandeis University, Waltham, Massachusetts 02453, USA
[3] Instituto de Ciencias de la Ingienería, Universidad O'Higgins, Rancagua, Chile
michael.berhanu@univ-paris-diderot.fr

Résumé. Un ensemble de particules granulaires vibrées magnétisées permet d'observer une transition entre un gaz granulaire et un cristal hexagonal dans un système 2D hors équilibre, lorsque le champ magnétique est augmenté à agitation constante [1]. En calculant, les fonctions de corrélation de courant longitudinal et transverse, nous étudions la dynamique de ce système en mesurant le spectre des excitations, indiquant comment l'énergie est répartie à travers les échelles. Des relations de dispersion peuvent être extraites, montrant la propagation d'ondes longitudinales et transverses (dans la phase cristalline seulement), qui sont analogues aux phonons de la physique du solide. Cette analyse nous informe sur les propriétés mécaniques et thermodynamiques du système.

Abstract. Using a 2D out-of-equilibrium system of magnetized and vibrated granular particles, a transition from a granular gas towards a hexagonal crystal has been reported, when magnetic field is increased at constant agitation [1]. By extracting the longitudinal and transverse current correlations in dynamical regime, the spectrum of excitations can be measured to characterize how energy is distributed through the scales. Dispersion relations are obtained, showing propagation of longitudinal waves and of transverse waves (in the crystal phase only), which are analogous to phonons in solid state physics. This analysis provides insights on the mechanical and thermodynamic properties of this system.

1 Introduction

A macroscopic experiment [1, 2] has been developed in MSC laboratory where a tunable magnetic field is applied on a 2D vibrated granular medium made of soft-ferromagnetic spheres. Like in condensed matter, depending on the relative ratio between particle agitation and distance interaction strength, gas-like or solid-like phases can be observed. They are characterized using a particle tracking of individual particles. For a specific choice of the initial particle number in the cell, of the cell acceleration and of the gap size imposing the 2D confinement, a transition from an out-of-equilibrium granular gas to a hexagonal crystal of repelling dipoles (analogous to the Wigner crystal) is observed, when the magnetic field is increased. The protocol, the description of the experimental system and the first results have been reported in a previous publication [1]. Here, we focus on the dynamical properties of this 2D granular system, studied in the spatial Fourier space. The computation of the transverse and longitudinal current correlation functions gives access to the spectrum of excitations and their temporal decay. We evidence strong differences between the dissipative granular gas phase and the hexagonal crystal phase.

The experimental setup (see Fig. 1) consists of an assembly of 2,000 soft magnetic spheres of diameter $a = 1$ mm confined in a square cell (9×9 cm) with a gap of $1.42\,a$. The cell is vertically vibrated at $f_v = 300$ Hz with a r.m.s. acceleration $\Gamma = 1.6\,g$. Due to the roughness of the cell bottom, the particles are performing Brownian-like motions in the horizontal plane. By imaging with a high speed camera on the area S_0 (5×5 cm) the trajectory of each particle is reconstructed. When the external vertical magnetic field B_0 is increased, each sphere behaves as an induced dipole. In first approximation, two particles separated by a distance $r_{i,j}$ interact according to the repulsive potential $U_{i,j} = \frac{4\pi}{\mu_0} B_0^2 \frac{(a/2)^6}{r_{i,j}^3}$. The parameters of our experiments are the area fraction $\phi = \frac{N\,\pi a^2}{4\,S_0}$ (with N the numbers of balls imaged on S_0), the mean kinetic energy per particle $E_c = \langle \frac{m}{2\,N} \sum_{i=1}^{N} v_i^2 \rangle$ (with m mass and velocity v_i of

particle i) and the mean magnetic energy per particle $E_\mathrm{m} = \langle \frac{1}{N} \sum_{i=1}^{N} \sum_{j=i+1}^{N} U_{i,j} \rangle$. The dimensionless number $\epsilon = E_\mathrm{m}/E_\mathrm{c}$ quantifies the ratio between interaction strength and kinetic energy. B_0 is varied in $[0.11, 430]$ G corresponding to $\epsilon \in [10^{-4}, 1.5 \times 10^3]$. Each run is repeated five times. After an equilibration time of 100 s, measurements are recorded during 3.85 s. As observed previously [1], in the center of the cell, the dimensionless particle density ϕ decreases with ϵ (Fig. 1 (b)), because particles are concentrating on the non repelling cell boundaries. The crystallization towards a hexagonal crystal is monitored by the hexagonal order parameter $|\Psi_6| = |\langle \frac{1}{n_k} \sum_{k=1}^{n_k} \mathrm{e}^{\mathrm{i}\, 6\theta_{jk}} \rangle|$ (the sum is performed on the angles of the first neighbours of one particle and averaged over the particles and over the time). $|\Psi_6|$ is of order 0.4 in the granular gas phase to reach 0.9 in the hexagonal crystal phase. The transition is located at $\epsilon \approx 62$ (Fig. 1 (c)), corresponding to a maximal susceptibility, of this order parameter.

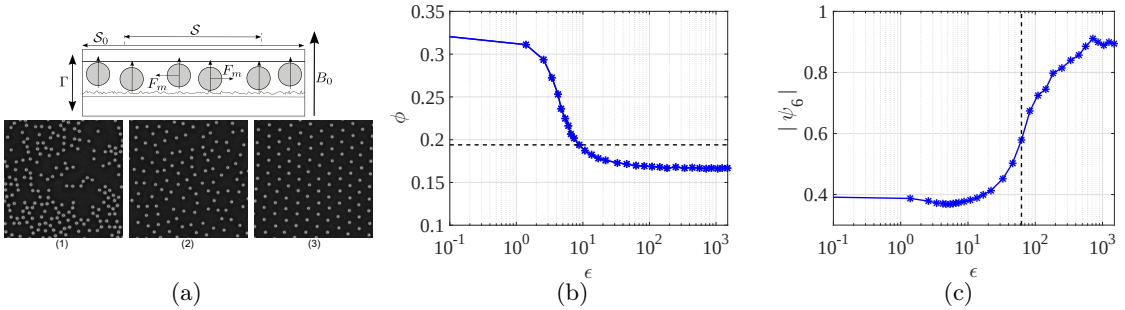

(a) (b) (c)

Figure 1. (a) Experimental setup. Snapshots (1) ($\epsilon \approx 0$), (2) ($\epsilon = 16.2$), (3) ($\epsilon = 283$). (b) Area fraction ϕ as a function of $\epsilon = E_\mathrm{m}/E_\mathrm{c}$. Dashed line, area fraction computed on the totality of the cell. (c) Hexagonal order parameter $|\Psi_6|$ versus ϵ. The black dashed line at $\epsilon = 62.4$ marks the transition between the granular phase and the hexagonal crystal phase.

To characterize how injected energy is transferred through the scales to build a stationary out-of-equilibrium state, a convenient method consists in studying the statistical properties of particle velocity field in spatial Fourier space. Velocity correlations at a particular wavenumber $\mathbf{k}$ appear naturally as a spectrum amplitude at the scale $\mathbf{k}$. We thus introduce the longitudinal current correlation function $J_l(\mathbf{k}, t)$ and the transverse current correlation function $J_t(\mathbf{k}, t)$, defined as [3, 4]:

$$J_l(\mathbf{k}, t) = \left\langle \frac{1}{N} \sum_{i,j=1}^{N} (\hat{\mathbf{k}} \cdot \mathbf{v}_i)(t)\, (\hat{\mathbf{k}} \cdot \mathbf{v}_j)(0)\, \mathrm{e}^{\,\mathrm{i}\mathbf{k}[\mathbf{r_i(t)} - \mathbf{r_j(0)}]} \right\rangle, \tag{1}$$

$$J_t(\mathbf{k}, t) = \left\langle \frac{1}{N} \sum_{i,j=1}^{N} (\hat{\mathbf{k}} \times \mathbf{v}_i)(t)\, (\hat{\mathbf{k}} \times \mathbf{v}_j)(0)\, \mathrm{e}^{\,\mathrm{i}\mathbf{k}[\mathbf{r_i(t)} - \mathbf{r_j(0)}]} \right\rangle. \tag{2}$$

$\hat{\mathbf{k}}$ is the unitary vector directed along $\mathbf{k}$. $\langle \cdot \rangle$ denotes a temporal average. These functions are computed on a grid (k_x, k_y) of size 50×50 on the interval $0.0624 < \|\mathbf{k}\| < 3.12$ mm^{-1}. Then assuming system isotropy, we define the angular averaged current correlation functions: $J_l(k, t) = (2\pi)^{-1} \int_0^{2\pi} J_l(\mathbf{k}, t)\, \mathrm{d}\theta$ and $J_t(k, t) = (2\pi)^{-1} \int_0^{2\pi} J_l(\mathbf{k}, t)\, \mathrm{d}\theta$.

2 Spatial spectra, distribution of energy over spatial scales

The values of $J_l(k, t)$ and $J_t(k, t)$ at $t = 0$, are respectively the structure factor of longitudinal velocity modes and of transverse velocity modes and can be interpreted as spatial power spectra as they

provide the kinetic energy distribution over the spatial scales. A flat spectrum as a function of k denotes equipartition of energy over the modes. Following the fluctuating hydrodynamics theory approach, for an out-of-equilibrium dissipative granular gas, $J_t(k \to 0, 0) = 2\,T_\mathrm{b}$ and $J_t(k \approx 2\pi/a, 0) = 2\,T_\mathrm{g}$ [4, 5], where T_b is the "bath" temperature and $T_\mathrm{g} \approx E_\mathrm{c}/m$ the usual granular temperature (these temperatures are defined by analogy with the physics of molecular systems). Due to the collisions at the grain size, in a dissipative granular gas, T_b is assumed larger than T_g. In our experiment, we observe that $J_t(k, 0)$ and $J_l(k, 0)$ are nearly flat (Fig. 2 (a)), except at the three smallest wavenumbers, where higher values are recorded. A plateau at large scale is not really visible maybe due to the lack of resolution in k. We measure the temperatures T_g as the average of $J_t(k, 0)$ on the five last values. The evolution of these temperatures as a function of ϵ are displayed in Fig. 2 (b) and compared with the usual granular temperature E_c/m. We find that $T_\mathrm{g} \approx E_\mathrm{c}/m$. As reported previously [1], we observe a non monotonous behavior of T_g, which is maximum for $\epsilon \approx 10$. Indeed, a moderate ϵ reduces the rate of dissipative collision. Then at higher amplitude of B_0, the formation of the hexagonal solid phase limits the horizontal displacements. In the hexagonal crystal phase, we remark that $J_t(k, 0)$ presents a smooth maximum around $k\,a \approx 1.5$. It is probably related to the propagation of the waves, which will be characterized in the following.

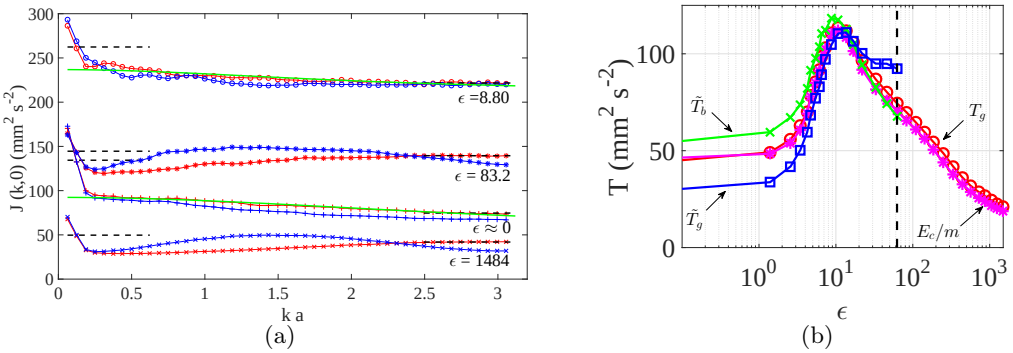

Figure 2. (a) Longitudinal spatial spectrum $J_l(k, 0)$ (blue) and transverse spatial spectrum $J_t(k, 0)$ (red) for few values of magnetic field B_0: (+) $B \approx 0$ G, $\epsilon \approx 0$, (∘) $B = 62$ G, $\epsilon = 8.80$, (∗) $B = 185$ G, $\epsilon = 83.2$ and (×) $B = 430$ G, $\epsilon = 1484$. For the two first cases, $J_t(k, 0)$ are fitted by the green line curves using Eq. (3). (b) Evolution of analog temperatures as a function of $\epsilon = E_\mathrm{m}/E_\mathrm{c}$. Red (∘) granular temperature T_g, Magenta (∗) E_c/m, Green (×) bath temperature $\tilde{T}_\mathrm{b}$ from fits of $J_t(k, 0)$ by Eq. (3) (see Sec. 3), Blue (□) granular temperature $\tilde{T}_\mathrm{g}$ from fit (Eq. (3)) only in the granular gas phase (see Sec. 3). The black dashed line at $\epsilon = 62.4$ marks the transition between the granular phase and the hexagonal crystal phase.

3 Decay of current functions. Characterization of dissipation.

To characterize the dissipative processes at play in the granular gas phase, we measure the temporal decay of the transverse current $J_t(k, t)$. In the granular gas phase, the decay is well approximated by a decreasing exponential $\sim \mathrm{e}^{-t/\tau(k)}$, where $\tau(k)$ is the typical lifetime of a perturbation at the scale k (Fig. 3 (a)). In vibrated granular layers, the dissipation is often modeled by the sum of a viscous drag and of a Coulomb friction: $\tau^{-1}(k) = \nu\,k^2 + \gamma_b$ [4], with ν a kinematic viscosity and γ_b a friction coefficient. This hypothesis appears valid in our measurements in the granular gas phase only. In the solid phase, the correlation functions are mainly oscillating and the exponential fits become questionable. ν rescaled by a^2 and γ_b are plotted as a function of ϵ in the granular gas phase ($0 < \epsilon < 62$) (Fig. 3 (b)). For this set of experiments, the dissipation appears dominated by the friction coefficient. A characteristic length $\xi = (\nu/\gamma_b)$ of order 0.3 mm can be defined. This value is considerably smaller than the one found in Puglisi et al. [4] (without magnetic interactions, without lid, for stronger agitation and for varying area

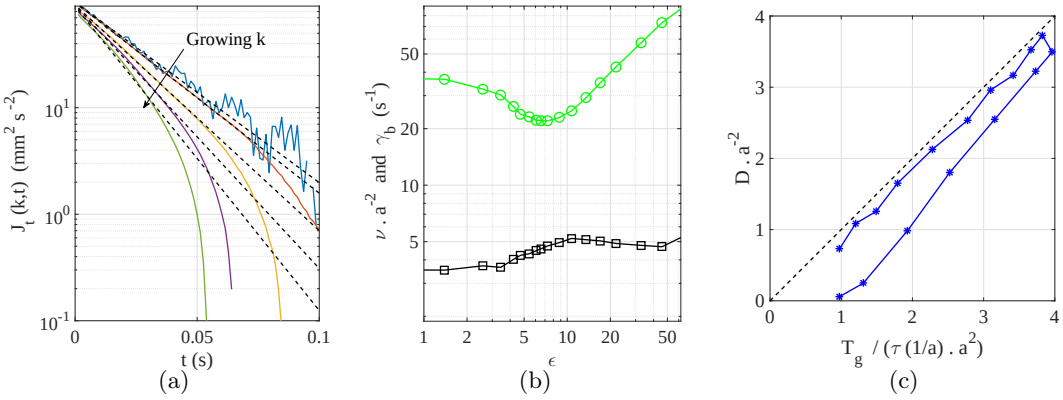

Figure 3. (a) Temporal decay of $J_{k,t}$, for various k (from top to bottom) for $\epsilon \approx 0$. Dashed line, corresponding to exponential fits defining the dissipative time $\tau(k)$. The behavior is similar for larger values of ϵ in the granular gas. (b) Evolution with ϵ of dissipative coefficients: green $\circ$ friction coefficient γ_b and black $\square$ rescaled kinematic viscosity ν/a^2. (c) Rescaled particles diffusion coefficient D/a^2 plotted as a function of $T_g/(\tau(1/a)\,a^2)$. Each point corresponds to a value of ϵ for $\epsilon < 62$. The dashed line is the line $y = x$.

fraction ϕ). The fluctuating hydrodynamics theory interprets this length as a spatial correlation length of excitations, which controls the shape of the transverse velocity structure factor $J_t(k,0)$ [4,5]:

$$\frac{J_t(k,0)}{2} = \tilde{T_g} + \frac{\tilde{T_b} - \tilde{T_g}}{1 + \xi^2\, k^2}. \tag{3}$$

In the granular gas phase, our measurements of $J_t(k,0)$ are well fitted by Eq. (3) (see Fig. 2 (a)), providing an estimation of the bath temperature $\tilde{T_b}$ and of granular temperature $\tilde{T_g}$. The difference $\tilde{T_b} - \tilde{T_g}$ quantifies the distance to the thermodynamic equilibrium [4,5]. In Fig. 2 (b), we compare as a function of ϵ these temperatures. The distance to equilibrium $\tilde{T_b} - \tilde{T_g}$ decreases with ϵ to vanish at $\epsilon = 17$ close to the maximum of T_g. Then $\tilde{T_g}$ becomes larger than $\tilde{T_b}$ denoting an inversion of the slope of $J_t(k,0)$. Due to the magnetic repulsion, large scale excitations become likely unfavorable. We note that $\tilde{T_g}$ differs from T_g and from the usual granular temperature E_c/m.

Finally, we examine briefly the link between diffusion and dissipation. The self-diffusion coefficients are obtained for each experiment by fitting the mean-square displacements of particles $\langle(\mathbf{r}_i(t) - \mathbf{r}_i(t = 0))^2\rangle = 4Dt$. The standard diffusion process remains valid in the granular gas phase until approximately $\epsilon < 50$. By analogy with the Einstein relation, we show experimentally:

$$\frac{D}{a^2} \approx \frac{T_g}{\tau(a^{-1})\,a^2} = \frac{E_c}{(\nu\, a^{-2} + \gamma_b)\, m\, a^2}. \tag{4}$$

This identity is particularly true for the points corresponding to the increase of T_g with ϵ and a little less when the system approaches the transition threshold. This result suggest that the fluctuation dissipation theorem holds in a dissipative granular gas, when the dissipation coefficients are estimated from the velocity correlation functions.

4 Spectra of excitations, dispersion relations

The dynamical properties of the system are now studied by computing the spatiotemporal velocity spectra in the wavenumber–frequency (k, f) space. From the Wiener–Khinchin theorem, the angular

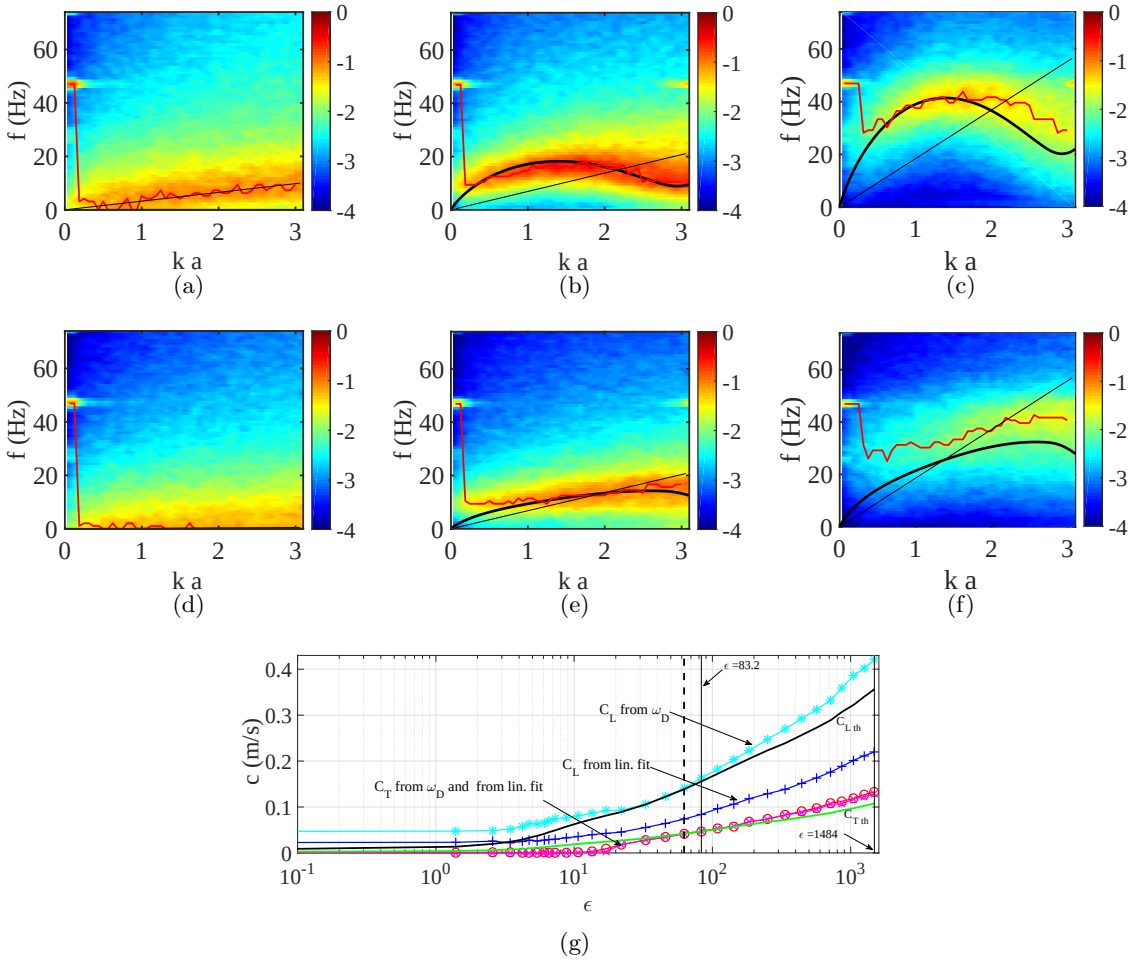

Figure 4. Longitudinal and transverse velocity spectra as a function of the rescaled wavenumber $k\,a$ and the frequency f. In colorscale $\log_{10}(S_v(k,f))$. (a) $S_{vl}(k,f)$ for $\epsilon \approx 0$. (b) $S_{vl}(k,f)$ for $\epsilon = 83.2$. (c) $S_{vl}(k,f)$ for $\epsilon = 1484$. (d) $S_{vt}(k,f)$ for $\epsilon \approx 0$. (e) $S_{vt}(k,f)$ for $\epsilon = 83.2$. (f) $S_{vt}(k,f)$ for $\epsilon = 1484$. Black thick line: theoretical dispersion relation for point dipoles [6]. Red line: experimental dispersion relation from local maxima. Black thin line: linear fit of experimental dispersion relation. (g) Experimental sound velocities extracted from the dispersion relations (see text). + blue, longitudinal, linear fit valid in the granular gas phase. ∘ red, transverse, linear fit. ∗ cyan, longitudinal sound velocity from experimental estimation of ω_D. × magenta, transverse sound velocity from experimental estimation of ω_D. Black C_{Lth} theoretical longitudinal sound velocity with the experimental parameters. Green C_{Tth} theoretical transverse sound velocity with the experimental parameters. Black dashed line at $\epsilon = 62.4$ the transition between the granular phase and the hexagonal crystal phase.

averaged velocity power spectra are deduced from the temporal current correlation functions by a Fourier transform:

$$S_{vl}(k,f) = \frac{1}{\sqrt{2\pi}} \int_0^T \int_0^{2\pi} J_l(\mathbf{k},t)\, k\, \mathrm{d}\theta\, \mathrm{e}^{2\mathrm{i}\pi f t}\, \mathrm{d}t \quad \text{and} \quad S_{vt}(k,f) = \frac{1}{\sqrt{2\pi}} \int_0^T \int_0^{2\pi} J_t(\mathbf{k},t)\, k\, \mathrm{d}\theta\, \mathrm{e}^{2\mathrm{i}\pi f t}\, \mathrm{d}t$$

Some typical longitudinal and transverse velocity spectra are displayed in Fig. 4 for $\epsilon \approx 0$ (granular gas), $\epsilon = 83.2$ (transition domain) and $\epsilon = 1484$ (hexagonal crystal). We notice in all measurements a strong peak around $f \approx 46$ Hz and $k \approx 0$. This global oscillation could be attributed to a vibration mode of the cell. In the granular gas phase, the maxima of $S_{vl}(k,f)$ when k is varied follows a line

crossing zero, defining a dispersion relation of compressive longitudinal waves (Fig. 4 (a)). In contrast, the maxima of $S_{vt}(k, f)$ are located in $f = 0$, revealing absence of transverse waves as expected in a fluid phase (Fig. 4 (d)). By increasing ϵ, as the system becomes more rigid, evidence of transverse waves dispersion appears (Fig. 4 (e) and 4 (f)). The dispersion relations differ from simple lines and become dispersive.

However, the dispersion relation of 2D system of point dipoles distributed in a hexagonal lattice can be analytically computed in the harmonic approximation (small displacements) [6]. In the solid phase, the theoretical dispersion relations are compatible with the experimental spectra. We note that at high ϵ, the large scales are not well energized, making a linear fit in this area questionable. To determine the sound velocity, which is given by $\frac{\partial \omega}{\partial k}$ when $k \to 0$, in the solid phase, we estimate the top of the experimental dispersion relations to get the characteristic pulsation ω_D. Theoretically, $\omega_D = \frac{B_0 \sqrt{2\,a}}{2\sqrt{m\,\mu_0\,\phi^{5/2}}}$ [6], then the longitudinal and transverse sound velocity read: $C_{\mathrm{Lth}} = \frac{1.283\,\omega_D\,a}{2\sqrt{\phi}}$ and $C_{\mathrm{Tth}} = \frac{0.387\,\omega_D\,a}{2\sqrt{\phi}}$. The corresponding experimental velocities ($*$ and $\times$) are reported in Fig. 4 (g) as a function of ϵ and compared to the theoretical estimates (black and green lines, valid only in the solid phase). Surprisingly, the agreement is better for moderate values of ϵ. The linearity of the sound velocities with B_0 (not displayed) is also well verified. The transverse sound velocity is zero in the granular gas phase and becomes non zero at $\epsilon = 17$, which is the beginning of the transition towards the hexagonal crystal phase and smaller than the threshold at $\epsilon = 62.4$ (maximal succeptibility of $|\Psi_6|$), which provides a supplemental criterion differentiating granular gas and crystal phases. The elastic coefficients could be then measured from the sound velocity estimations without perturbing the system.

5 Conclusion

The dynamical analysis of this system provides a good macroscopic illustration of phenomenon usually observed in solid state physics. In the granular phase, energy is mediated by compression longitudinal waves, whereas in the hexagonal solid phase, energy transfers between particles occur by the equivalent of phonons, whose dispersion relations can be analytically computed. Similar observations have been reported in hexagonal crystal of charged particles (dusty plasmas) [7], with a different interaction potential. The main difference with microscopic systems is the out-of-equilibrium character of our experiment. In the granular gas phase, the fluctuating hydrodynamic theory explains well the deviation from energy equipartition due to the dissipation. As ϵ increases in the granular gas phase, we quantify the decrease of the distance to equilibrium as it was stated in our previous work [1] for the quasi-elastic phase.

Acknowledgements : We thank Thierry Hocquet and Martin Devaud for using their computing facilities at MSC. This research was supported by Fondecyt Grant No. 3160032 (G.C.).

References

1. S. Merminod, M. Berhanu & É. Falcon, Transition from a dissipative to a quasi-elastic system of particles with tunable repulsive interactions, *Europhys. Lett.*, **106**, 44005 (2014).
2. S. Merminod, T. Jamin, É. Falcon & M. Berhanu, Transition to a labyrinthine phase in a driven granular medium, *Phys. Rev. E*, **92**, 062205 (2015).
3. G. Castillo, *Order and density fluctuations in the vicinity of a granular solid–liquid-like phase transition*, Phd Thesis, Universidad de Chile (2013).
4. A. Puglisi, A. Gnoli, G. Gradenigo, A. Sarracino & D. Villamaina, Structure factors in granular experiments with homogeneous fluidization, *J. Chem. Phys.*, **136**, 014704 (2012).
5. G. Gradenigo, A. Sarracino, D. Villamaina & A. Puglisi, Non-equilibrium length in granular fluids: From experiment to fluctuating hydrodynamics, *Europhys. Lett.*, **96**, 114004 (2011).
6. K. I. Golden, G. J. Kalman, P. Hartmann & Z. Donko, Dynamics of two dimensional dipole systems, *Phys. Rev. E*, **82**, 036402 (2010).
7. S. Nunomura, S. Zhdanov, D. Samsonov & G. Morfill, Wave spectra in solid and liquid complex (dusty) plasmas, *Phys. Rev. Lett.*, **94**, 045001 (2005).